Bubble Detection on the Cathode and Anode of a High-Performing Capillary-Fed Water Electrolysis Cell

Anh Linh Hoang,[1] Rhodri E. Owen,[2] George Tsekouras,[1] Dan J. L. Brett,[2,] Gerhard F. Swiegers[1,3,*]*

[1] Intelligent Polymer Research Institute, University of Wollongong, Wollongong, NSW 2522, Australia

[2] Electrochemical Innovation Lab, Department of Chemical Engineering, University College London. Gower Street, London, WC1E 6BT, United Kingdom

[3] Australian Research Council Centre of Excellence for Electromaterials Science, University of Wollongong, Wollongong, NSW 2522, Australia

[*] Corresponding Author Emails: d.brett@ucl.ac.uk, swiegers@uow.edu.au

Abstract:

The cathode and anode of a 'bubble-free' 'capillary-fed' water electrolysis cell that was previously reported to consume only 40.4 kWh kg^{-1} hydrogen under standard commercial operating conditions, have been separately investigated for the incidence of gas bubble formation during operation. Adaptions of a voltage fluctuation and an acoustic emission technique were applied in combination, to detect and analyze bubble formation at current densities up to 1 A cm^{-2}. The two techniques produced very similar results, showing little bubble formation up to 0.17-0.20 A cm^{-2}. Thereafter, bubbles were formed predominantly at the cathode up to ~0.6 A cm^2. At higher current densities, the cathode and anode produced bubbles at similar rates, that were substantially lower than in conventional, 'bubbled' electrolysis cells. In the course of this work, the previously reported high electrochemical performance of the capillary-fed cell was independently confirmed.

1.   Introduction

In conventional water electrolysis cells, hydrogen and oxygen gas are produced from liquid water on the electrodes, in the form of bubbles. Gas bubble formation involves a process of nucleation and growth, followed by detachment of the bubble from the electrode surface. During that process, the bubbles create a so-called *'bubble curtain'* that covers the surface of the electrode, blocking electrolyte access by the liquid electrolyte and increasing the resistance between the electrodes.[1-4] As a consequence, the energy efficiency of the electrolysis cell is decreased.

To minimize the negative effect of gas bubbles, many conventional alkaline and polymer electrolyte membrane (PEM) electrolysers continuously pump liquid electrolyte over

2

their electrode surfaces to dislodge and remove gas bubbles.[1,3,5] However, this introduces additional energy losses and extra costs to the system due to the energy consumption of the pumps and the additional piping, vessels, and engineering equipment required, as well the maintenance for such equipment.

It has historically proved challenging to accurately determine the overpotential due to bubble formation in water electrolysis. Vogt and colleagues examined the fraction of an electrode surface that was covered by gas bubbles during operation under different conditions.[1,3,6,7] They found that bubble coverage increased with increasing current density and temperature in 3 M KOH electrolyte at ambient pressure in stagnant electrolyte.[6] At above 1.0 A cm^{-2}, the bubble coverage became excessive, notably decreasing the active surface area of the electrode.[7] Flowing liquid electrolyte over the electrode significantly decreased the bubble coverage with the fractional coverage dependent on the velocity of flow.[1]

In early 2019, Li *et al*.[8] reported a 'breathable' oxygen-evolving anode that was prepared by sputter coating a thin gold layer onto a porous, hydrophobic polyethylene (PE) membrane, followed by electrodepositing a NiFeO$_x$ catalyst onto the gold layer. The 'breathable' nature of the electrode derived from the fact that the resulting NiFeO$_x$/Au/PE electrode produced oxygen from water without producing visible gas bubbles at room temperature; the oxygen was drawn, as it was generated, through the porous PE membrane into a gas chamber at its rear. In so doing, the electrode exhibited a 90 mV lower overpotential at 0.01 A cm^{-2} than when a non-porous PE substrate was used. The non-porous PE substrate forced the formation of oxygen bubbles as no pathway existed to extract the gas from the NiFeO$_x$ catalyst layer and this is why it displayed a higher overpotential.

At around the same time, Tiwari *et al*.[9] reported a comparison between a 'bubble-free' cell employing Gortex gas diffusion electrodes and conventional, bubble-generating electrolysis cells. They calculated that the contribution of bubble formation to the activation

overpotential was ~0.16 V at 80 °C, excluding the effect of impedance. The energy efficiency decrease caused by bubble formation in conventional, bubble-generating electrolysers was estimated to be ≥11.9% (vs. the Lower Heating Value, LHV, of hydrogen).

Most recently, a novel class of 'bubble-free' electrolysis cell, known as a *capillary-fed* cell, has been developed.[10] In such cells, the gases are produced in bulk form directly from the liquid electrolyte that lightly, but completely, coats the electrodes. A thin, wicking separator between the electrodes draws the alkaline liquid electrolyte up to the electrodes from a reservoir at the base of the cell. The electrodes, which are sandwiched tightly against opposite sides of the separator in a zero-gap configuration, draw small amounts of liquid electrolyte laterally out of the separator causing them to be completely covered with only a thin layer of the liquid electrolyte. The gas formed on the electrode surface can then migrate through the thin layer of liquid electrolyte into an adjoining gas chamber, without forming gas bubbles. The outcome of this arrangement is that the energy efficiency of the cell is significantly improved. Indeed, a capillary-fed water electrolysis cell has been reported that requires only 40.4 kWh to produce 1 kg of hydrogen under the standard operating conditions employed in many commercial alkaline electrolyzers.[10] This supersedes the efficiency target of <42 kWh kg^{-1} set by the *International Renewable Energy Agency* (IRENA) for the year 2050.[10]

While the above capillary-fed cell is essentially bubble-free at low current densities, some gas bubbles are produced at higher current densities. This is likely because one or both electrodes become overhydrated; that is the layer of liquid electrolyte on the surface of the electrodes becomes too thick. For example, water is produced at the oxygen-generating anode in alkaline electrolysis cells. At higher current densities the quantity of water produced in the capillary-fed alkaline cell may conceivably thicken the liquid layer on the anode, slowing the migration of the oxygen gas product into its gas chamber and leading to the formation of some

4

bubbles. Understanding the processes that occur at each electrode and their relationship with the current density is critical to further improvements in energy efficiency.

To achieve the necessary insights, suitable interrogation and measurement techniques are needed to detect what occurs on each electrode surface. High-speed video cameras have commonly been used as a non-invasive tool to monitor gas evolution on electrode surfaces.[11-14] However, it is extremely difficult, if not physically impossible, to observe bubble generation in a zero-gap cell using a high-speed camera, even in the form of a boroscope.[15-17] Therefore, it is necessary to develop other techniques that could be applied to the detection and characterization of bubble formation in water electrolysers.

Acoustic emission has been demonstrated as a cost-effective, non-destructive testing technique that can detect and monitor transition elastic waves produced under the stress of material deformation. It is generally deployed in structural testing, process monitoring and materials characterisation.[18] This technique has been gaining attention for its potential applications in electrochemical devices [ref] and has been applied to the detection of bubble formation in PEMWE by monitoring and analyzing sound waves generated when bubbles form and burst.[19-21] However, its use and technical capabilities in 'bubble-free' or 'bubble-scarce' electrolysers have not been studied.

Recently, Tsekouras *et al*.[10,22] also introduced a novel technique with which to electrochemically observe bubble formation in electrolysis cells. This approach analyzes, at high resolution, the standard deviation of the voltage fluctuations that occur in electrolysis cells at fixed current densities. The process of bubble nucleation, growth, coalescence, and release on an electrode induces large voltage fluctuations because gas bubbles constitute non-conducting voids that transiently block the access of the liquid electrolyte to the electrode surface. By contrast, 'bubble-free' gas generation involves almost negligible voltage fluctuations as the electrode surface is always fully in contact with the liquid electrolyte.

Commented [OR1]: https://iopscience.iop.org/article/10.1088/2515-7655/abfb4a/meta

5

Accordingly, the standard deviation, σ, of the voltage profile of water electrolysis at a fixed current density can be used as a proxy for bubble formation. While powerful, this approach has only been applied to electrolysis cells, meaning that bubble formation on the individual electrodes in an operating cell has not been investigated.

This work describes two new adaptions of the above techniques, applied in combination, to separately detect and analyze bubble formation on the anode and cathode in a capillary-fed cell. In the course of this work, the electrochemical performance of the alkaline capillary-fed water electrolysis cell that was reported to require only 40.4 kWh kg^{-1} hydrogen under standard commercial operating conditions,[10] was also independently corroborated at the Electrochemical Innovation Laboratory at University College London. Results are provided.


2. Results and Discussion

2.1 Electrochemical Analysis of the Anode and Cathode of a *Capillary-fed* Electrolysis Cell

2.1.1 Experimental Setup and Procedures

To separately investigate the anode and cathode of a 2-electrode capillary-fed cell during water electrolysis, it was necessary to introduce a reference electrode into the system. This was done by preparing a transparent, acrylic, second-generation test cell of the same type described previously,[10] and then cutting off its bottom, as depicted in Figure 1. The transparency of the cell allowed for viewing inside during operation; however, little could be observed, requiring the need for the more advanced techniques reported here.

6

The cell was then assembled in a zero-gap configuration, with a cathode and anode sandwiched tight up against opposite sides of a fast-wicking polyethersulfone (PES) separator membrane with 8 μm average pore diameter ('8 μm PES'). The bottom end of the PES separator extended out the bottom of the cell, as shown in the exploded view in Figure 1.
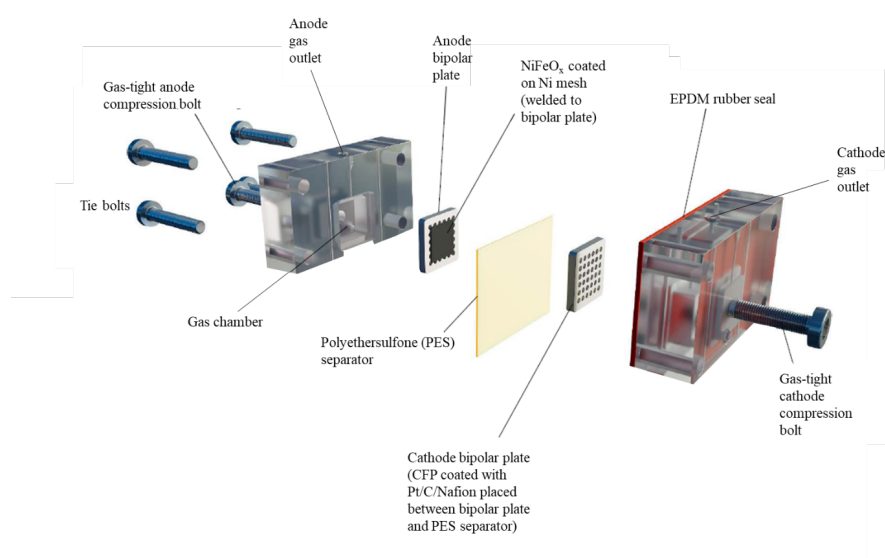
Figure 1. Exploded view of the transparent, acrylic second-generation test cell with its bottom cut off.

The cathode comprised a Pt/C catalyst with 26 wt% Nafion binder (*vs.* total solids in the catalyst slurry) sprayed onto a Sigracet carbon paper gas diffusion layer (GDL) substrate until it had a net loading of 0.5 mg cm^{-2} Pt. The cathode was prepared using the preparative procedure of Hodges and co-workers,[10] which was based on one previously reported by Masel and colleagues.[21] The cathode is designated in this work as: 'Pt/C/Nafion/CFP'. It was maintained in direct electrical contact with a perforated Ni bipolar plate and a gas-tight cathode

compression bolt, by screwing in the compression bolt, as shown in Figure 1. After assembly of the cell, a torque of 25 N cm was applied to the compression bolt to compress the Ni bipolar plate against the cathode, which was then, in turn, compressed against the PES separator.

The anode comprised a $NiFeO_x$ layer that was electrodeposited to incorporate PTFE particulates, onto a fine Ni mesh anode as described by Hodges *et al.*;[10] this procedure was based on previous work by Benedetti and co-workers.[23] The anode is designated here as 'NiFeO$_x$/PTFE/Ni mesh'. The anode Ni mesh electrode was spot welded to its perforated Ni bipolar plate as previously described.[10] The Ni bipolar plate was maintained in direct electrical contact with a gas-tight anode by screwing in a compression bolt, as shown in Figure 1. After assembly of the cell, a torque of 25 N cm was applied to the compression bolt to compress the Ni bipolar plate and attached welded anode against the PES separator.

The 8 μm PES had previously been shown to be capable of supplying liquid electrolyte to the electrodes at a sufficient rate to operate the cell continuously and at high current density.[10] The 8 μm PES separator membrane has a mildly asymmetric pore profile across its thickness. One side has fewer and smaller pores (the 'gloss' side) than the other side (the 'matt' side).[10] As conventional alkaline electrolysis cells are generally known to produce smaller bubbles of hydrogen than oxygen,[24,25] the gloss side of the separator membrane was placed facing the hydrogen-generating cathode with the matt side facing the oxygen-generating anode.

The cell, thus assembled, was then placed on a stand in a large beaker that was one-third filled with aqueous 6 M KOH (which we called a 'reservoir beaker'). This allowed the bottom end of the 8 μm PES separator membrane to dip into the KOH solution while the rest of the cell remained above the liquid level. Figure 2 schematically illustrates this arrangement.

8
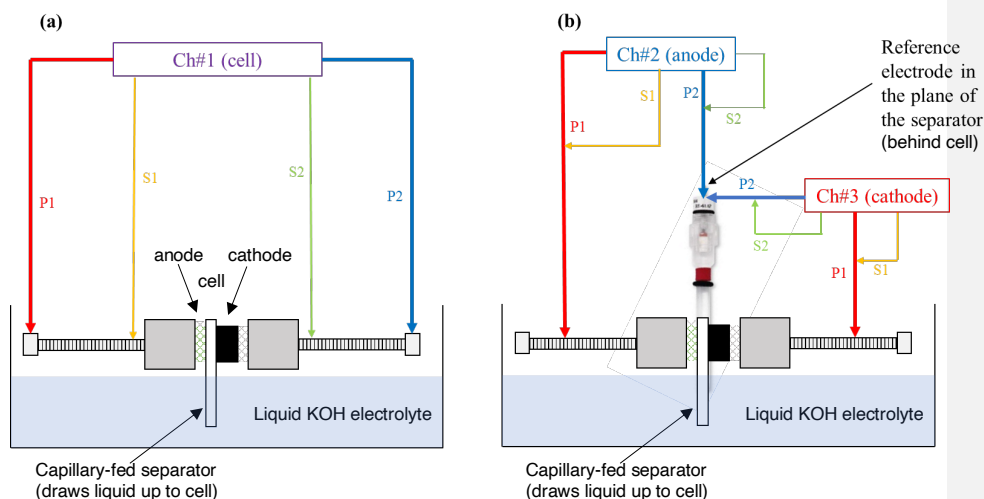
Figure 2. Schematic of arrangement of the second-generation test cell in Figure 1 in a 'reservoir beaker' containing 6 M KOH. Image (a) and (b) schematically illustrate three electrical circuits that were created by connecting three potentiostat channels to the cell. (a) The circuit denoted 'Ch#1 (cell)' shows the 4-wire connection of the first potentiostat channel to the compression bolts of the cell; this connection was used to drive water electrolysis in the cell. (b) The circuit denoted 'Ch#2 (anode)' shows the connection of the second potentiostat channel to the reference electrode and the anode compression bolt, while the circuit denoted 'Ch#3 (cathode)' shows the connection of the third potentiostat channel to the reference electrode and the cathode compression bolt. The latter two electrical circuits were used to monitor the anode and cathode respectively. (P = power lead, S = sense lead).

To simultaneously investigate the anode and cathode, as well as the cell voltage, a Hg/HgO reference electrode was dipped into the 6 M KOH in the beaker in the plane of the separator. Three channels of a Biologic VSP-300 potentiostat were then attached to the cell to create three separate electrical circuits, as shown in Figure 2(a)-(b).

The first circuit connected the first potentiostat channel via a 4-wire connection, to the two gas-tight compression bolts, whose ends pressed against and made electrical contact with their respective bipolar plates (Figure 2(a); 'Ch#1 (cell)')). This first circuit was used to drive

water electrolysis within the cell; that is, it formed the primary electrochemical system during operation of the cell.

Reservoir containing liquid electrolyte (6 M KOH)

Hg/HgO reference electrode
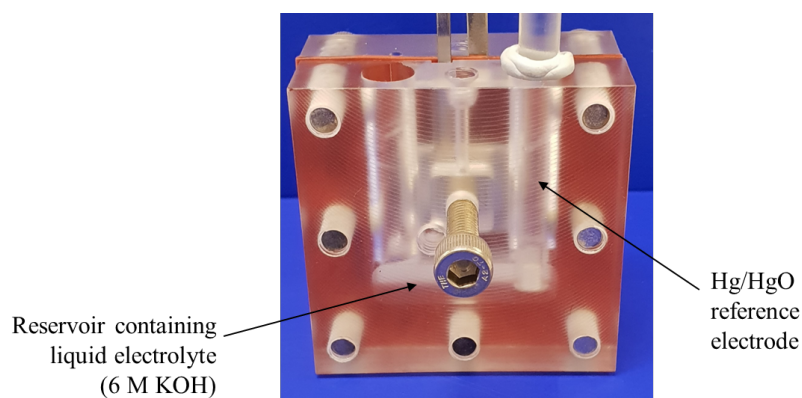
Figure 3. Photograph showing an alternative adaption of the transparent, acrylic second-generation test cell for this study. A 6 cm wide cavity was drilled from the top of one half-cell into the reservoir cavity of the cell. A Hg/HgO reference electrode was then placed in the cavity so that its end was immersed in the liquid in the reservoir.

The two further circuits were created to monitor the electrochemical performance of each of the anode and the cathode. One of these circuits connected the second potentiostat channel to the reference electrode and anode compression bolt (Figure 2(b); 'Ch#2 (anode)'), while the other connected the third potentiostat channel to the reference electrode and the cathode compression bolt (Figure 2(b); 'Ch#3 (cathode)'). To avoid side reactions and CO_2 uptake by the KOH electrolyte, the beaker headspace was maintained and filled with an inert Ar atmosphere.

An adaption of the above cell arrangement could, alternatively, be used, albeit with caveats. A transparent, acrylic second-generation cell of the above type was modified by drilling a 6 mm wide hole from the top of the cell to the electrolyte reservoir cavity as shown in Figure 3. A Hg/HgO reference electrode was then introduced into the resulting cavity, such

10

that its active end was immersed in the liquid electrolyte in the reservoir. The electrical connections were then made as described above, with the cell or its contents maintained under an inert Ar atmosphere.

A disadvantage of this alternative arrangement was that even moderate evaporation during an experiment could change the molarity of the KOH electrolyte, thereby changing the area-specific resistance (ASR) between the electrodes and altering the cell performance. Nevertheless, the cell could be used successfully if experiments were carried out quickly and carefully. A set-up similar to this, with the reference electrode holes excluded, was used for all acoustic emission testing.

After allowing the cell, in one of the above experimental arrangements, to stand for several hours, steady-state chronopotentiometry was carried out by stepping up the current density delivered by the first (cell) potentiostat channel in the order: 10, 20, 30, 40, 50, 75, 100, 125, 150, 175, 200, 250, 300, 350, 400, 450, 500, 600, 700, 800, 900, and 1,000 mA cm^{-2}, where each step was held for 20 s. The two other (anode, cathode) potentiostat channels were set to record the open-circuit voltage (OCV) at the anode and cathode relative to the Hg/HgO reference electrode during this process. This voltage data was collected in high resolution, at a rate of 5 data points per second. The resulting voltage data was then converted to the equivalent voltages vs. the reversible hydrogen electrode (RHE) using the equation $E_{RHE} = E_{Hg/HgO} + (0.0592 \times pH) + 0.118$ (pH = 14.7 corresponding to 6 M KOH).

Current-voltage plots for each of the anode and cathode were obtained by averaging the voltage measured at the anode and cathode respectively, in the last 10 s of each of the above 20 s steps.

In accordance with the voltage fluctuation technique described previously,[10] the standard deviation, σ, of the voltage data at each of the anode and cathode was calculated over the last 10 s of each 20 s step period and plotted against the respective current density. Low

11

values of σ were typically associated with bubble-free gas generation (e.g. less than σ ~0.2 mV), while higher values (e.g. more than σ ~0.2 mV) were consistent with bubble formation.

For acoustic emission studies, all electrochemical tests were conducted using an Interface 5000 potentiostat (Gamry, U.S.A.) with the electrical connections set-up as shown in Figure 2(a). Data obtained for both set-ups were found to match closely with similar polarization curves and voltage fluctuation measurements. For the acoustic emission experiments, the data were collected following the same procedure as that used for the voltage fluctuation experiments with the exception of the timings for each step. Each current step was held for 60 s with 120 s rest periods between. This increase in time allowed for more statistically significant acoustic emission data to be collected.

A cylindrical 8 mm diameter piezoelectric transducer was used to collect acoustic emission data (Nano30, Mistras NDT, U.K.) with an operating frequency range of 125-750 kHz. Good contact between the transducer and the Pyrex body of the electrolyser was ensured through the use of high-temperature acoustic couplant (Couplant H-2, Olympus, Japan). The transducer was placed over the center top part of the current collection plate and held in place with electrical tape. The transducer was connected to a 1283 USB AE node acoustic emission system (MISTRAS, U.S.) with the data collected and analyzed using AEwin software (MISTRAS, U.S.). A noise threshold of 25 dB was used for all data collection to distinguish between background noise and what was classified as an acoustic hit. The high acoustic impedance of the EPDM gasket between the two halves of the cell allows for the acoustic behavior of the anode and cathode to be decoupled to some extent and the electrode under study selected by swapping the side of the cell that the transducer is in contact with. Tests were repeated with no couplant and a small distance between the sensor and the body of the cell. These tests gave no acoustic hits, confirming that any signals observed while the test was running were not due to any potential electromagnetic interference.

12
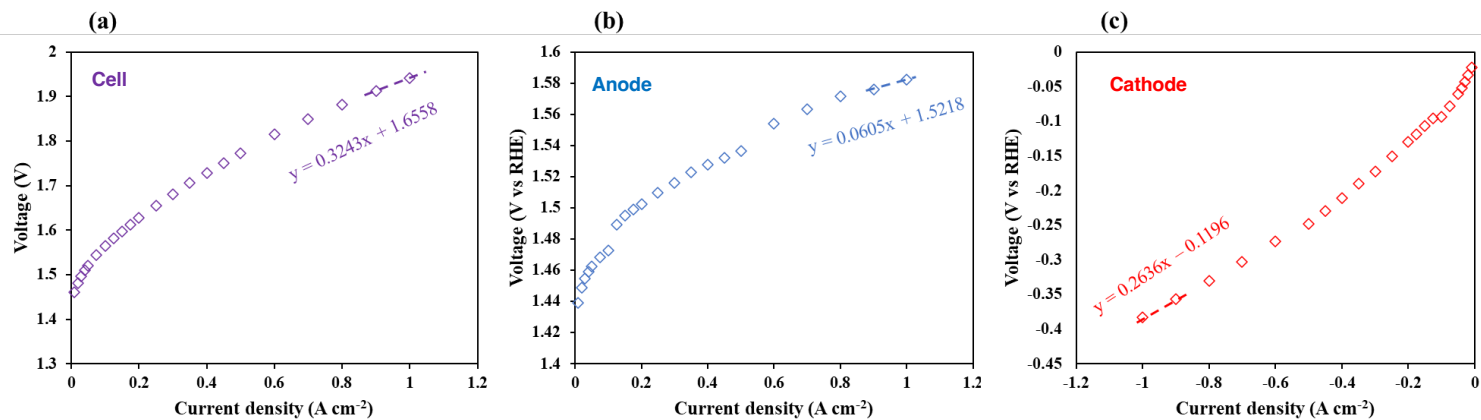
Figure 4. Voltage - current profiles derived from steady-state chronopotentiometry, as a function of current density, at room temperature (23 °C), of the capillary-fed electrolysis cell with a Pt/C/Nafion/CFP (0.5 mg cm^{-2} Pt) cathode and NiFeO$_x$/PTFE/Ni mesh anode:[10] (a) Overall cell voltage. (b) Voltage at the anode. (c) Voltage at the cathode. Electrolyte: 6 M KOH.

Table 1. Selected room temperature (23 °C) performance metrics of the cell in Figure 4.

	Onset potential (V *vs.* RHE)	Overpotential (mV)			Cell / electrode resistance (Ohmic slope at 1 A cm^{-2}) (mΩ cm^2)
		at 0.1 A cm^{-2}	at 0.5 A cm^{-2}	at 1.0 A cm^{-2}	
Overall cell	1.524	333	542	712	324
Anode	1.480	240	294	329	61
Cathode	0.046	93	248	383	263

13

All acoustic and voltage fluctuation experiments were conducted at room temperature (23 °C).

2.1.2 Current-Voltage Plots of the Anode and Cathode of a *Capillary-Fed* Electrolysis Cell

Figure 4 shows the voltage *vs* current density plots derived from steady-state chronopotentiometry measurements of: the overall cell (Figure 4(a)), the anode (Figure 4(b)), and the cathode (Figure 4(c)). Selected performance metrics are listed in Table 1.

As can be seen, the onset potential (vs. RHE) of the cell was 1.460 V, of which 1.439 V originated in the anode and 0.021 V derived from the cathode.

The cell resistance was 324 mΩ cm^2, of which the anode contributed a surprisingly low 61 mΩ cm^2 while the cathode contributed a much higher 263 mΩ cm^2. Thus, while the anode had a notably higher onset potential than the cathode, consistent with the more sluggish nature of the oxygen-evolution reaction (OER) relative to the hydrogen-evolution reaction (HER), it produced far smaller increases in voltage as the current density increased, than the cathode.

Thus, in going from a current density of 0.1 A cm^{-2} to 0.5 A cm^{-2} to 1 A cm^{-2}, the overpotential at the anode changed from 240 mV to 294 mV to 329 mV; a total increase of 89 mV. By contrast, the overpotential at the cathode changed, in the same sequence, from 93 mV to 248 mV to 383 mV; a total increase of 290 mV. Accordingly, the performance of the cell was dominated by the anode at low current densities, but increasingly by the cathode at high current densities.

Given that the carbon fiber paper (CFP) at the cathode was specified to have a resistance of <10 mΩ cm^2 and the contact resistance at the cathode was previously found to be only 3-5 mΩ cm^2, this raises a question about the origin of the high, 263 mΩ cm^2 resistance at the

14

cathode. To try to answer that question, the formation of gas bubbles at the cathode and anode as a function of current density was examined.

2.1.3 Gas Bubble Detection at the Anode and Cathode of the *Capillary-Fed* Electrolysis Cell using the Voltage Fluctuation Technique

From the steady-state chronopotentiometry measurements, the standard deviation (σ) of voltage was calculated and plotted against current density, as shown in Figure 5. Selected data are listed in Table 2. In accordance with the voltage fluctuation technique, both the absolute values of the standard deviation and their trends, serve as measures of bubble formation.

As can be seen in Figure 5, for all of the cell, the anode, and the cathode, the plots reveal two profiles (shown by the dashed lines); namely, a region with relatively flat σ values (at low current densities) and a region of modestly increasing σ values (at higher current densities). The former region indicates largely bubble-free operation.[10] The latter region indicates substantially but not completely bubble-free operation (relative to conventional bubbled cells).[10]

What is notable in these plots is that, whereas the anode is largely bubble free at current densities up to ~0.3 A cm^{-2}, the cathode is largely bubble free only up to ~0.17 A cm^{-2}. Moreover, while the overall upward trend of bubble formation at the cathode at higher current densities (dashed line (i)) in Figure 5(c)) has a similar slope to that of the anode, a notably steeper sub-trend can be seen in the cathode data at intermediate current densities (dashed line (ii) in Figure 5(c)).

15
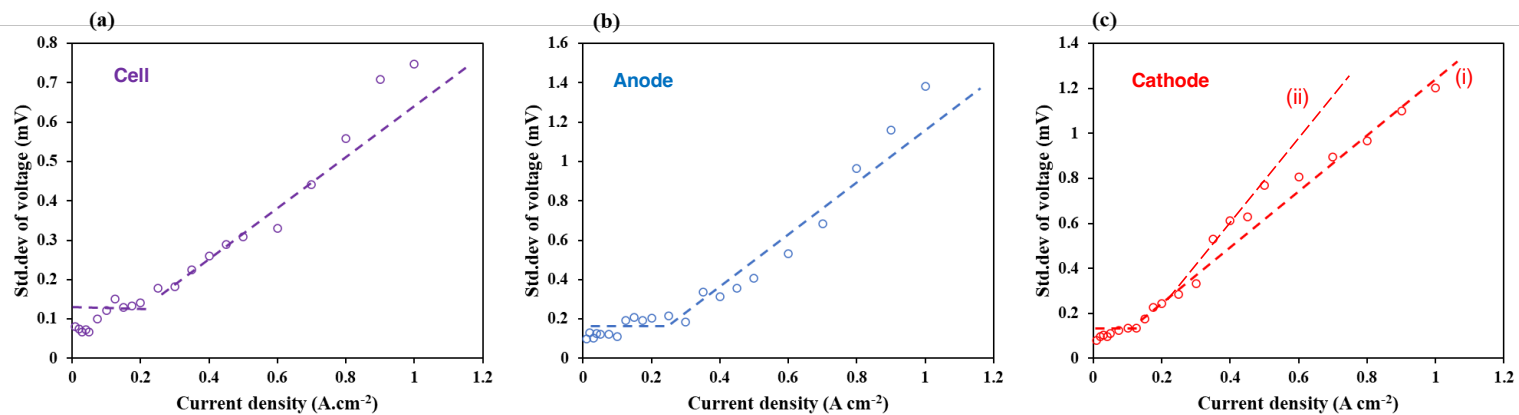
Figure 5. Standard deviation (σ) of voltage as a function of current density, at room temperature (23 °C), of: (a) the cell, (b) the anode, and (c) the cathode, of a capillary-fed water electrolysis cell with a Pt/C/Nafion/CFP cathode (0.5 mg cm^{-2} Pt) and NiFeO$_x$/PTFE/Ni mesh anode sandwiched in a zero-gap arrangement with a 8 μm PES membrane that fed 6 M KOH electrolyte to the electrodes from a reservoir at the base of the cell.

Table 2. Selected room temperature (23 °C) performance metrics of the cell in Figure 5.

	Standard deviation (σ) (mV)				
	at 0.01 A cm^{-2}	at 0.1 A cm^{-2}	at 0.4 A cm^{-2}	at 0.6 A cm^{-2}	at 1.0 A cm^{-2}
Overall cell	0.08	0.12	0.26	0.32	0.75
Anode	0.10	0.11	0.31	0.53	1.38
Cathode	0.08	0.14	0.61	0.80	1.20

Thus, bubble formation is indicated to be far more prevalent at the cathode than the anode in the region $0.3 - 0.6$ A cm^{-2}. Indeed, all bubble formation in the range $0.17 - 0.3$ A cm^{-2} is at the cathode and almost all bubble formation in the range $0.3 - 0.6$ A cm^{-2} is at the cathode.

This is significant insofar as most commercial alkaline electrolysers operate in the latter current density range, which provides the best compromise of capital costs (capex) and operating costs (opex) for alkaline electrolysis. If comparisons are to be made of the capillary-fed cell with commercial alkaline electrolysers at current densities in this range, then the key opportunity for further performance improvements in the capillary-fed cell lies in minimizing bubble formation at the cathode.

The sub-trend referred to above can be clearly seen in the selected data in Table 2. Whereas similar standard deviations are observed at 0.01 A cm^{-2} and 0.1 A cm^{-2} for the anode and cathode (σ 0.08-0.14), the σ value of the cathode is roughly double that of the anode at 0.4 A cm^{-2} (σ 0.61 vs 0.31) and ~50% larger at 0.6 A cm^{-2} (σ 0.80 vs 0.53).

Another interesting feature of the data is that the voltage signal noise (σ) was generally lower for the cell than for the anode or cathode alone (as demonstrated by the data in Table 2). This may potentially be explained by a degree of noise cancellation (i.e. voltage fluctuations at the anode combined with voltage fluctuations at the cathode that results in a lower overall standard deviation for the cell).

The voltage signal noise at the anode in the flat σ region up to 0.2 A cm^{-2} (Figure 5(b)) was also noticeably lower than that at the cathode (Figure 5(c)). There was more bubble formation on the cathode than the anode in the region of $0.2 - 0.8$ A cm^{-2}, which is consistent with the higher resistance at the cathode. In the region between $0.9 - 1.0$ A cm^{-2}, the voltage signal noise on the anode and the cathode was comparable.

Commented [BD2]: Should standardise on the use of the em or en dash for denoting range throughout the paper

Commented [GS3R2]: Standardised with the Em dash. GS

At 1 A cm^{-2}, the cell displayed a standard deviation of σ 0.75 mV (Table 2). This is significantly less than the σ 3.10 mV reported previously for a comparable, conventional bubbled cell, and was equivalent to around 9% of the current going into production of gas in the form of bubbles.[10]

2.1.4 Gas Bubble Detection at the Anode and Cathode of the *Capillary-Fed* Electrolysis Cell using the Acoustic Emission Technique

In addition to the voltage fluctuation measurements, acoustic emission testing was employed to monitor bubble formation on the anode and cathode sides of the cell separately. Although this work was conducted on a cell with a slightly different layout, as outlined in Section 2.1.1, results from both set-ups were found to match closely (See Figure SI 5).

The results obtained from acoustic emission testing are summarized in Figure 6. The use of the highly acoustically attenuating EPDM gasket between the two halves of the electrolyser allowed for the acoustic effects from each of the electrodes to be effectively isolated from one another. However, the crossover between electrodes was shown to be minimal.

Constant current steps (60 s) of increasingly high areal current density were conducted with 120 s rests between each value. The acoustic emission was monitored across the course of the experiment. The results in Figure 6 indicated that every time an acoustic event (a 'hit') was detected, it was above the chosen threshold value of 25 dB. The amplitude of each hit is indicated in each plot.

For the cathode (Figure 6 (a)) very few acoustic hits were observed at low current densities (e.g. only two hits were observed across the 1 min, 10 mA cm^{-2} period), this is an indication of exceptionally low bubble formation with very limited acoustic activity. This trend

for low amounts of bubble formation at low areal current densities continued across the first few current densities tested, although notably as the current density increased there was an increase in the number of hits occurring in each constant current step. After approximately 1500 s the number of acoustic hits increased more significantly. It is also observed that while there are hits just above the 25 dB threshold across the course of the experiment, increasing numbers of hits at higher acoustic amplitudes were observed as the current density increased.

Notably, no acoustic activity is observed during any of the rest steps even at higher current densities, this indicated that the acoustic behavior is related to the operation of the electrolyser and not due to any background effects. Tests were also repeated with the transducer in the same location but acoustically decoupled from the cell; no hits were detected during this test, ruling out any possible electromagnetic interference effects.

This result suggests a change in behavior as the current density is increased, in line with the results observed from voltage fluctuation measurements. More acoustic activity is attributable to the formation of bubbles.

The same experiment was repeated with the transducer placed on the anode of the electrolyser, these results are shown in Figure 6(b). A similar trend is observed at the anode as the cathode; namely, at lower current densities there is limited acoustic activity, indicating low bubble formation, which gradually increases as the areal current density is increased. If the number of hits recorded at the anode (Figure 6(b)) is compared to the number of hits recorded under the same conditions at the cathode (Figure 6(a)), fewer hits are observed at each current density, suggesting lower acoustic activity indicating lower bubble formation. These results correlate with the data obtained from voltage fluctuation experiments, which indicated that bubble formation was more prevalent at the cathode than the anode.

19
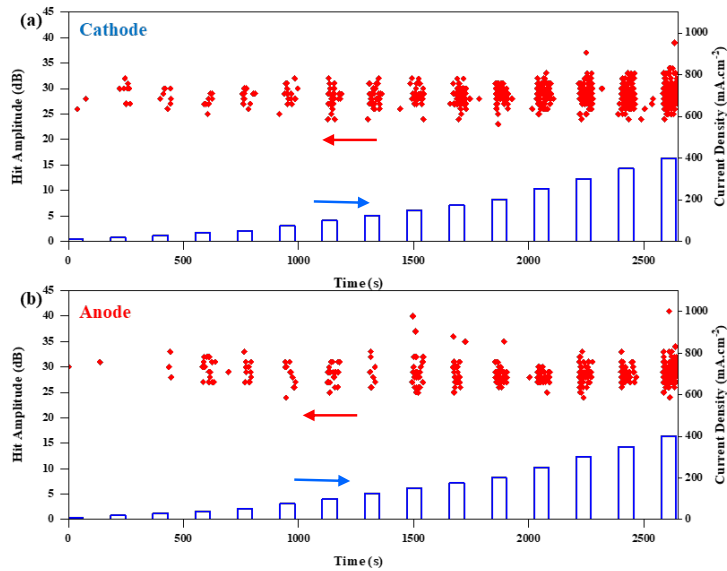
Figure 6. Acoustic emission data obtained from (a) cathode side and (b) anode side as current density (blue bars) (right axis) is increased and acoustic results (red dots) show the hit amplitude (left axis) and rate. Note that there are no acoustic hits in the current rest periods.

In order to compare the acoustic activity at the anode and cathode at all current densities studied, the hit rate (number of hits per second) was calculated for all areal current values on both electrodes, the data from these calculations are shown in Figure 7(a). During periods of low areal current density, both the anode and the cathode show relatively low acoustic activity indicating a low rate of bubble formation, corroborating the data obtained in the voltage fluctuation measurements. However, when the current density is increased above the 0.2 – 0.3 A cm^{-2} range there is an increase in the rate of increase of acoustic hits per second at the cathode with increasing current density, suggesting more bubble formation; this is a similar trend to that observed with the voltage fluctuation experiments. The results obtained for the anode indicate that this transition to a higher gradient occurs at higher current densities in the region

of $0.3 - 0.4$ A cm^{-2}, this again correlates well with the voltage fluctuation measurements reported.

At current densities above *ca.*. 75 mA cm^{-2} the hit rate for the cathode is always higher than that observed at the anode, indicating more prevalent bubble formation at the cathode. At higher current densities, above the 0.2-0.3 A cm^{-2} range, this difference in acoustic activity increases further with a higher gradient observed with the cathode relative to the anode (Figure 7 (a)). This again matches well with results obtained from voltage fluctuation experiments.
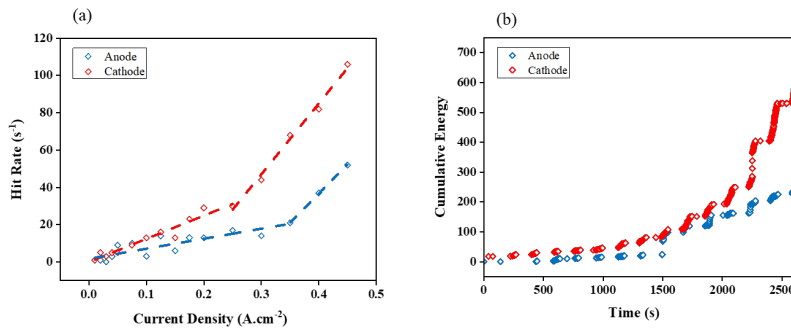
Figure 7. (a) The acoustic hit rate for both the anode and cathode at varying areal current densities. (b) the evolution of the cumulative energy across the course of the test for both the anode and cathode.

This difference between the higher acoustic activity observed with the cathode relative to the anode, particularly at current densities above 0.2-0.4 A cm^{-2} is more clearly observed by studying the cumulative energy of the acoustic hits (Figure 7(b)). Thus far, the focus has been on the number of hits recorded, which gives a good indication of the acoustic activity but does not include all information contained within each acoustic hit. By looking at the cumulative energy, this not only takes into account the total number of hits but other factors associated with each hit such as the duration and frequency of each hit. The measurement of cumulative energy has previously been used to great effect to study and understand the performance of fuel

cells.[ref] Based on the cumulative energy the performance of the two electrodes is relatively similar, albeit with the cathode showing slightly higher energy, until approximately 1500 s. At this point, where the current density is increased beyond 0.2 A cm^{-2}, there is a more significant deviation between the cathode and anode. These results match closely with the voltage fluctuation experiments indicating that bubble formation is more prevalent at the cathode and for higher current densities above *ca.* 0.2 A cm^{-2} the effect is initially larger on the cathode than the anode.

2.1.5 Statistical Correlation of the Acoustic Emission Technique and the Voltage Fluctuation Technique

To assess how well the acoustic technique correlated with the voltage fluctuation technique as a means of detecting gas bubble formation, correlations plots were constructed.
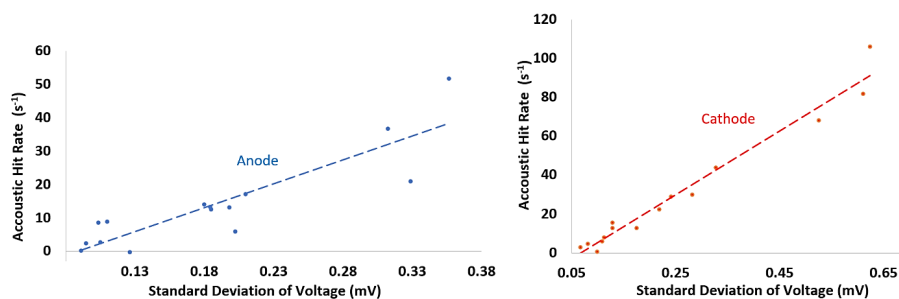
Figure 8. Correlation plots of the acoustic hit rate (from Figure 7(a)) and the standard deviation arising from voltage fluctuations (from Figure 4(b)-(c)) for: (a) the anode, and (b) the cathode.

Figure 8(a) and Figure 8(b) depict the statistical correlation of the acoustic hit rates (from Figure 7(a)) and the standard deviations due to voltage fluctuations (from Figures 4(b)-(c)), at current densities up to 0.45 A cm^{-2}, for the anode and cathode, respectively. The graphs

indicate that there is a significant positive relationship between the acoustic hit rate and the standard deviation arising from voltage fluctuations for both the anode and the cathode. The anode (Figure 8(a)) demonstrates a Pearson correlation $r(13) = 0.884$ with a P-value of $P < 0.001$. The cathode (Figure 8(b)) displays a Pearson correlation $r(13) = 0.984$ with a P-value of $P < 10^{-10}$. Both correlations are statistically significant, with P-values below 0.05.

Accordingly, the acoustic and voltage fluctuation techniques provide essentially identical trends in respect of gas bubble formation and are statistically equally reliable in this respect.

3.   Conclusions

In this work, we have detected and analyzed the incidence of gas bubble formation during operation, of the cathode and anode of a high-performing capillary-fed water electrolysis cell. A voltage fluctuation and an acoustic emission technique were adapted and applied in combination, while applying current densities of up to 1 A cm^{-2} to the cell. Very similar results were obtained for the two techniques, with little bubble formation observed up to 0.17-0.20 A cm^{-2}. At higher current densities, up to around 0.6 A cm^{-2}, bubbles were formed predominantly at the cathode. Given that commercial alkaline electrolysers typically operate at current densities up to 0.6 A cm^{-2}, this suggests that minimizing bubble formation at the cathode offers the key opportunity for further performance improvements in the capillary-fed cell. The cathode and anode produced bubbles at similar rates at still higher current densities, to 1 A cm^{-2}. Even at 1 A cm^{-2}, the rate of bubble formation on the electrodes was substantially lower than in conventional, 'bubbled' electrolysis cells. Correlation plots indicated that the acoustic and voltage fluctuation techniques demonstrated statistically significant positive correlations for both the cathode and the anode, with P-values below 0.001 (anode) and 10^{-10} (cathode). In the

23

course of this work, the previously reported high electrochemical performance of the capillary-fed cell was independently confirmed.

References

1.   Balzer, R. J.; Vogt, H., Effect of Electrolyte Flow on the Bubble Coverage of Vertical Gas-Evolving Electrodes. *J. Electrochem. Soc.* **2003**, *150* (1), E11-E16.

2.   Dukovic, J.; Tobias, W. C., The Influence of Attached Bubbles on Potential Drop and Current Distribution at Gas-Evolving Electrodes. *J. Electrochem. Soc.: Electrochemical Science and Technology.* **1987**, *134* (2), 331.

3. Eigeldinger, J.; Vogt, H., The Bubble Coverage of Gas-Evolving Electrodes in a Flowing Electrolyte. *Electrochim. Acta.* **2000**, *45* (2000), 4449-4456.

4. Zeng, K.; Zhang, D., Recent Progress in Alkaline Water Electrolysis for Hydrogen Production and Applications. *Prog. Energy Combust. Sci.* **2010**, *36* (3), 307-326.

5. Wang, M.; Wang, Z.; Gong, X.; Guo, Z., The Intensification Technologies to Water Electrolysis for Hydrogen Production – A Review. *Renew. Sust. Energ. Rev.* **2014**, *29*, 573-588.

6. Vogt, H.; Balzer, R. J., The Bubble Coverage of Gas-Evolving Electrodes in Stagnant Electrolytes. *Electrochim. Acta.* **2005**, *50* (10), 2073-2079.

7. Vogt, H., The Actual current Density of Gas-Evolving Electrodes—Notes on the Bubble Coverage. *Electrochim. Acta.* **2012**, *78*, 183-187.

8. Li, J.; Zhu, Y.; Chen, W.; Lu, Z.; Xu, J.; Pei, A.; Peng, Y.; Zheng, X.; Zhang, Z.; Chu, S.; Cui, Y., Breathing-Mimicking Electrocatalysis for Oxygen Evolution and Reduction. *Joule.* **2019**, *3* (2), 557-569.

9. Tiwari, P.; Tsekouras, G.; Wagner, K.; Swiegers, G. F.; Wallace, G. G., A New Class of Bubble-Free Water Electrolyzer that is Intrinsically Highly Efficient. *Int. J. Hydrog. Energy.* **2019**, *44* (42), 23568-23579.

10. Hodges, A.; Hoang, A. L.; Tsekouras, G.; Wagner, K.; Lee, C.-Y.; Swiegers, G. F.; Wallace, G. G., A High-Performance Capillary-Fed Electrolysis Cell Promises more Cost-Competitive Renewable Hydrogen. *Nat. Commun.* **2022**, *13* (1), 1304.

11. Glas, J. P.; Westwater, J. W., Measurements of the Growth of Electrolytic Bubbles. *In. J. Heat Mass Transfer.* **1964**, *7* (1427-1443).

12. Brussieux, C.; Viers, P.; Roustan, H.; Rakib, M., Controlled Electrochemical Gas Bubble Release from Electrodes Entirely and Partially Covered with Hydrophobic Materials. *Electrochim. Acta.* **2011**, *56* (20), 7194-7201.

13. Davis, J. T.; Brown, D. E.; Pang, X.; Esposito, D. V., High Speed Video Investigation of Bubble Dynamics and Current Density Distributions in Membraneless Electrolysers. *J. Electrochem. Soc.* **2019**, *166* (4), F312-F321.

14. Ikeda, H.; Misumi, R.; Kojima, Y.; Haleem, A. A.; Kuroda, Y.; Mitsushima, S., Microscopic High-Speed Video Observation of Oxygen Bubble Generation Behavior and Effects of Anode Electrode Shape on OER Performance in Alkaline Water Electrolysis. *Int. J. Hydrog. Energy.* **2022**, *47* (21), 11116-11127.

15. Wendt, H.; Hofmann, H., Cermet Diaphragms and Integrated Electrode-Diaphragm Units for Advanced Alkaline Water Electrolysis. *Int. J. Hydrog. Energy.* **1985**, *10* (6), 375-381.

16. Phillips, R.; Dunnill, Charles W., Zero Gap Alkaline Electrolysis Cell Design for Renewable Energy Storage as Hydrogen Gas. *RSC Adv.* **2016,** *6* (102), 100643-100651.

17. Nakajima, Y.; Fujimoto, N.; Hasegawa, S.; Usui, T., Advanced Alkaline Water Electrolyzer for Renewable Hydrogen Production. *ECS Trans.* **2017**, *80* (10), 835-841.

18. Scruby, C. B., An Introduction to Acoustic Emission. *J. Phys. E: Sci. Instrum.* **1987,** *20*, 946.

19. Husin, S.; Addali, A.; Mba, D., Feasibility Study on the Use of the Acoustic Emission Technology for Monitoring Flow Patterns in Two Phase Flow. *Flow. Meas. Instrum.* **2013**, *33*, 251-256.

20. Maier, M.; Meyer, Q.; Majasan, J.; Tan, C.; Dedigama, I.; Robinson, J.; Dodwell, J.; Wu, Y.; Castanheira, L.; Hinds, G.; Shearing, P. R.; Brett, D. J. L., Operando Flow Regime Diagnosis Using Acoustic Emission in a Polymer Electrolyte Membrane Water Electrolyser. *J. Power Sources.* **2019**, *424*, 138-149.

21. Maier, M.; Meyer, Q.; Majasan, J.; Owen, R. E.; Robinson, J. B.; Dodwell, J.; Wu, Y.; Castanheira, L.; Hinds, G.; Shearing, P. R.; Brett, D. J. L., Diagnosing Stagnant

Gas Bubbles in a Polymer Electrolyte Membrane Water Electrolyser Using Acoustic Emission. *Front. Energy Res.* **2020**, *8*, 582919.

22. Tsekouras, G.; Terrett, R.; Yu, Z.; Cheng, Z.; Swiegers, G. F.; Tsuzuki, T.; Stranger, R.; Pace, R. J., Insights into the Phenomenon of 'Bubble-Free' Electrocatalytic Oxygen Evolution from Water. *Sustain. Energy Fuels.* **2021**, *5* (3), 808-819.

23. Sakita, A. M. P., Vallés, E., Noce, R. D. & Benedetti, A. V. Novel NiFe/NiFe-LDH Composites as Competitive Catalysts for Clean Energy Purposes. *Appl. Surf. Sci.* **2018**, *447*, 107–116.

24. Janssen, L. J. J.; Sillen, C. W. M. P.; Barendrecht, E.; van Stralen, S. J. D., Bubble Behaviour during Oxygen and Hydrogen Evolution at Transparent Electrodes in KOH Solution. *Electrochim. Acta* **1984**, *29* (5), 633-642.

25. Matsuura, K.; Yamanishi, Y.; Guan, C.; Yanase, S., Control of Hydrogen Bubble Plume during Electrolysis of Water. *J. Phys. Commun.* **2019**, *3* (3).

Bubble Detection on the Cathode and Anode of a High-Performing Capillary-Fed Water Electrolysis Cell

*Anh Linh Hoang,[1] Rhodri E. Owen,[2] George Tsekouras,[1] Dan J. L. Brett,[2,*] Gerhard F. Swiegers[1,3,*]*

Independent Replication at University College London (UCL), of the Performance of the Capillary-Fed Electrolysis Cell, as reported in *Nature Communications* 2022, *13*, 1304 (DOI: 10.1038/s41467-022-28953-x) by the University of Wollongong (UOW)

For acoustic emission testing carried out at University College London (UCL) a different set-up (as detailed in Section 2.2 of the manuscript) was utilised. In order to ensure that the data obtained from these tests was valid and matched data recorded at the University of Wollongong (UOW), previously reported experiments were repeated and the data compared. Figure SI 1 (a) shows a polarization curve obtained from the cell operating at 80 °C following the procedures outlined in Ref [1]. Figure SI 1 (b) shows a comparison of the data obtained in this work (measured at UCL) with the data reported previously in Ref [1]. The test was repeated at 85 °C with the results shown in Figure SI 2.
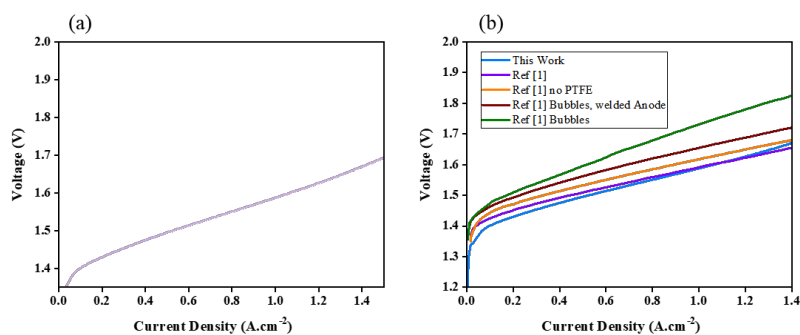

Figure SI 1. The polarisation curve obtained at 80 °C at UCL as part of this work (a) and compared to the previously reported work conducted at UOW (Ref [1]).
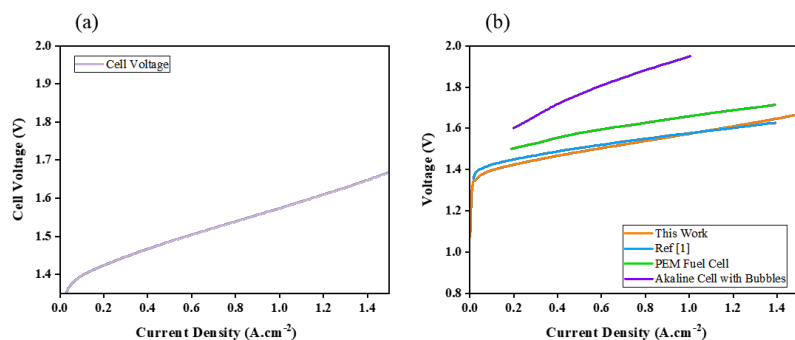
Figure SI 2. The polarisation curve obtained at 85 $^\circ$C at UCL as part of this work (a) and compared to the previously reported work conducted at UOW (Ref [1]).

To ensure cell stability was also maintained, the cell was operated at 85 $^\circ$C and a current density of 294 mA.cm^{-2} for over 40 mins with no reduction in performance observed as shown in Figure SI 3.
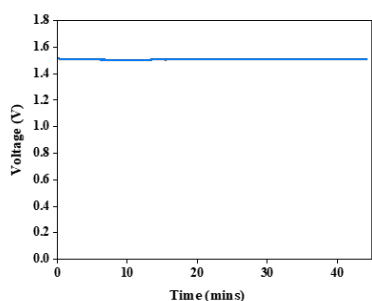

Figure SI 3. The voltage stability observed for a cell operating at 294 mA.cm^{-2} at 85 $^\circ$C.

Cell voltage values obtained at several previously reported current densities (Ref [1]) were replicated and showed good correlation with the previously reported values (Figure SI 4 (a)-(b)).
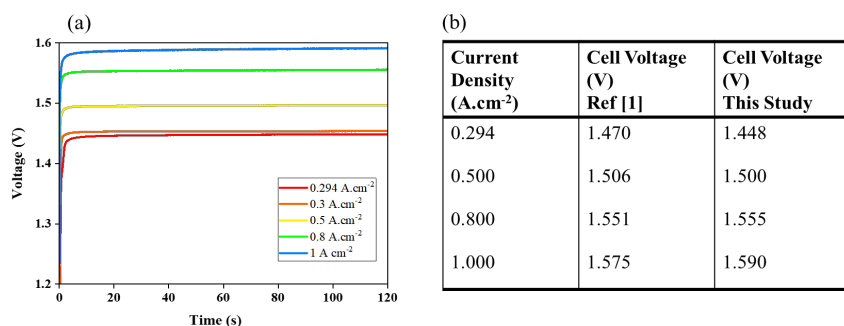
Figure SI 4. Recorded cell voltages at various current densities for a capillary-fed cell operating at 85 ºC.

With this study focusing on the perfomance of the cell at room temperature, several of the experiments conducted at UOW that are included in this mauscript were repeated at UCL. A good correlation between the tests carried out at each universiy on each set-up was observed as shown in Figure SI 5.
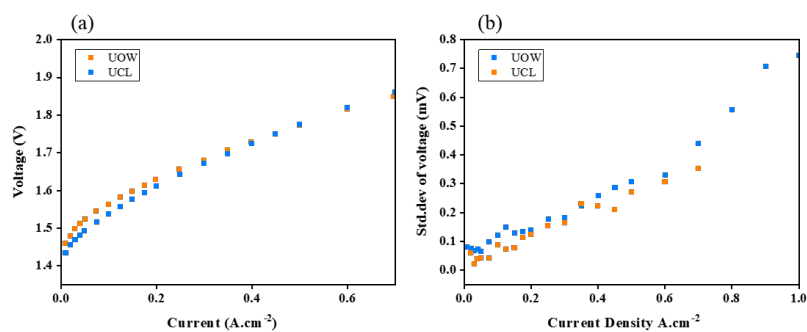
Figure SI 5. A comparison between the room temperature experimental data collected at UCL and the UOW: (a) voltage – current plots of the capillary-fed electrolysis cell, and (b) plots of the standard deviation of voltage at fixed current densities of the capillary-fed electrolysis cell (as described in section 2.1.2-2.1.3 of the manuscript).

The volume of hydrogen and oxygen generated at room temperautre with an areal current of 350 mA.cm^{-2} was found to match closely with theoretical values expected if the faradaic efficiency was 100%, see Figure SI 6.
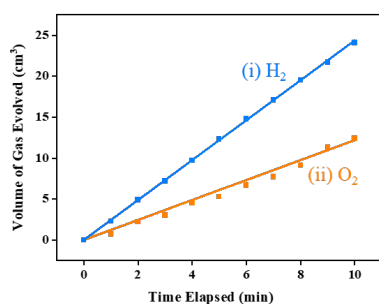
Figure SI 6. The measured volume of hydrogen and oxygen (dots) produced at room temperature and an areal current of 350 mA.cm^{-2} compared to theoretical values (solid lines)

References (Supplementary Material only)

[1]   Hodges, A.; Hoang, A. L.; Tsekouras, G.; Wagner, K.; Lee, C.-Y.; Swiegers, G. F.; Wallace, G. G., A High-Performance Capillary-Fed Electrolysis Cell Promises more Cost-Competitive Renewable Hydrogen. *Nat. Commun.* **2022**, *13* (1), 1304.